Supplemental Document

Optics EXPRESS

Tight-focusing parabolic reflector schemes for petawatt lasers: supplement

SIMON VALLIÈRES,[1,†,*] FRANÇOIS FILLION-GOURDEAU,[2,3,†] STÉPHANE PAYEUR,[3] JEFFREY POWELL,[3] SYLVAIN FOURMAUX,[3] FRANÇOIS LÉGARÉ,[3] AND STEVE MACLEAN[1,2,3]

[1] *Institute for Quantum Computing, University of Waterloo, 200 University Ave. W., Waterloo, Ontario N2L 3G1, Canada*
[2] *Infinite Potential Laboratories, 485 Wes Graham Way, Waterloo, Ontario N2L 0A7, Canada*
[3] *INRS-EMT, 1650 Blvd. Lionel-Boulet, Varennes, Québec J3X 1P7, Canada*
[†] *Equivalent first-author contributions*
[*] *simon.vallieres@uwaterloo.ca*

Supplement DOI: https://doi.org/10.6084/m9.figshare.22689928

Parent Article DOI: https://doi.org/10.1364/OE.486230

Tight-Focusing Parabolic Reflector Schemes for Petawatt Lasers: Supplementary Material

Simon Vallières[1,†,*], François Fillion-Gourdeau[2,3,†], Stéphane Payeur[3], Jeffrey Powell[3], Sylvain Fourmaux[3], François Légaré[3] and Steve MacLean[1,2,3]

[1] *Institute for Quantum Computing, 200 University Ave W., Waterloo, Ontario, Canada, N2L 3G1*
[2] *Infinite Potential Laboratories, 485 Wes Graham Way, Waterloo, Ontario, Canada, N2L 0A7*
[3] *INRS-EMT, 1650 blvd. Lionel-Boulet, Varennes, Québec, Canada, J3X 1P7*
[†] *Equivalent first-author contributions*
[*] *simon.vallieres@uwaterloo.ca*

1. NA calculation

In order to better compare the geometries, it is necessary to carefully calculate the Numerical Aperture (NA) of the tight-focusing reflectors. The NA is a metric that evaluates the range of angles from a light cone of an optic, defined as:

$$\mathrm{NA} = \sin\theta_{\max}\,, \tag{S1}$$

where $\theta_{\max}$ is the maximum angle the focusing half-cone of light. Depending on the geometry, the NA must be evaluated using the proper approach, otherwise yielding erroneous results. In the following sections, the NA will be evaluated for the three parabolic geometries presented in this work.

1.1. HNAP

We first find the maximum radius with $r_{\max} = D/2$. Then, considering the space margin Δ, we find the focal length f_0 as:

$$z_{\max} = \frac{r_{\max}^2}{4f_0} - f_0 = -\Delta \qquad \Longrightarrow \qquad f_0 = \frac{1}{2}\left(\Delta + \sqrt{\Delta^2 + r_{\max}^2}\right)\,. \tag{S2}$$

We can then find the maximum focusing angle $\theta_{\max}$ using:

$$\theta_{\max} = \arctan\left(\frac{r_{\max}}{-z_{\max}}\right) = \arctan\left(\frac{r_{\max}}{f_0 - \dfrac{r_{\max}^2}{4f_0}}\right)\,. \tag{S3}$$

Finally, the NA of the reflector is found using the conventional relationship:

$$\mathrm{NA} = \sin\theta_{\max} = 0.999\,. \tag{S4}$$

1.2. OAP90

We first find the two extrema radii as:

$$r_{\min} = \Delta \qquad \text{and} \qquad r_{\max} = \Delta + D\,. \tag{S5}$$

Using offset distance of the central ray $d_{\mathrm{offset}} = \Delta + D/2$ and the off-axis angle θ_{off}, we can find the effective focal distance f_{eff} and then f_0 using the conventional relationships for OAPs:

$$f_{\mathrm{eff}} = \frac{d_{\mathrm{offset}}}{\sin\theta_{\mathrm{off}}} \qquad \text{and} \qquad f_0 = \frac{2 f_{\mathrm{eff}}}{1+\cos\theta_{\mathrm{off}}} \,. \tag{S6}$$

The two extrema angles are further found using:

$$\theta_{\mathrm{min,\,max}} = \arctan\left(\frac{r_{\mathrm{min,\,max}}}{-z_{\mathrm{min,\,max}}}\right) = \arctan\left(\frac{r_{\mathrm{min,\,max}}}{f_0 - \dfrac{r^2_{\mathrm{min,\,max}}}{4 f_0}}\right) . \tag{S7}$$

For an OAP, the rotational symmetry is not around the longitudinal axis but rather around the segment of the central ray after the reflection, from the parabola to the focus. It is important note here that it defines a cone of light around the central ray with its half-angle defined by $\theta_{\mathrm{OAP}} = \Delta\theta/2 = (\theta_{\mathrm{max}} - \theta_{\mathrm{min}})/2$. Finally, we find the NA using:

$$\mathrm{NA} = \sin\left(\frac{\theta_{\mathrm{max}} - \theta_{\mathrm{min}}}{2}\right) = 0.867\,. \tag{S8}$$

1.3. TP

For the case of a cone of light with a hole, it is necessary to adopt a different approach since the NA is not additive due to the sin function, and therefore we cannot subtract the NA of the hole directly. For a given obstruction ratio $\alpha = (D_{\mathrm{in}}/w_{\mathrm{FWHM}})^2 = (2r_{\mathrm{min}}/w_{\mathrm{FWHM}})^2$, we first find the two extrema radii as:

$$r_{\mathrm{min}} = \frac{w_{\mathrm{FWHM}}}{2}\sqrt{\alpha} \qquad \text{and} \qquad r_{\mathrm{max}} = D/2\,. \tag{S9}$$

We then find the focal length f_0 as:

$$z_{\mathrm{min}} = \frac{r^2_{\mathrm{min}}}{4 f_0} - f_0 = \Delta \qquad \Longrightarrow \qquad f_0 = \frac{1}{2}\left(\sqrt{\Delta^2 + r^2_{\mathrm{min}}} - \Delta\right) . \tag{S10}$$

The two extrema angles are further found using:

$$\theta_{\mathrm{min,\,max}} = \arctan\left(\frac{r_{\mathrm{min,\,max}}}{-z_{\mathrm{min,\,max}}}\right) = \arctan\left(\frac{r_{\mathrm{min,\,max}}}{f_0 - \dfrac{r^2_{\mathrm{min,\,max}}}{4 f_0}}\right) . \tag{S11}$$

Then, as opposed to the NA, it is crucial to note that the solid angles of different light cones are additive. Considering a light cone Ω with half-angle θ having a solid angle of $\Omega = 2\pi\,(1-\cos\theta)$, we can write:

$$\mathrm{NA} = \sin\left[\arccos\left(1 - \frac{\Omega}{2\pi}\right)\right] . \tag{S12}$$

Using the above expression, we can generalize the NA evaluation for any kind of geometrical incidence by integrating the total solid angle over the sphere, and then evaluating the NA as a single equivalent light cone. For the case of the TP, this gives:

$$\Omega_{\mathrm{TP}} = \int_0^{2\pi}\int_{\theta_{\mathrm{min}}}^{\theta_{\mathrm{max}}} \sin\theta\,\mathrm{d}\theta\mathrm{d}\phi = 2\pi\,(\cos\theta_{\mathrm{min}} - \cos\theta_{\mathrm{max}}) \,, \tag{S13}$$

which finally yields:

$$\mathrm{NA} = \sin\left[\arccos\left(1 - \frac{\Omega_{\mathrm{TP}}}{2\pi}\right)\right] = 0.938\,. \tag{S14}$$

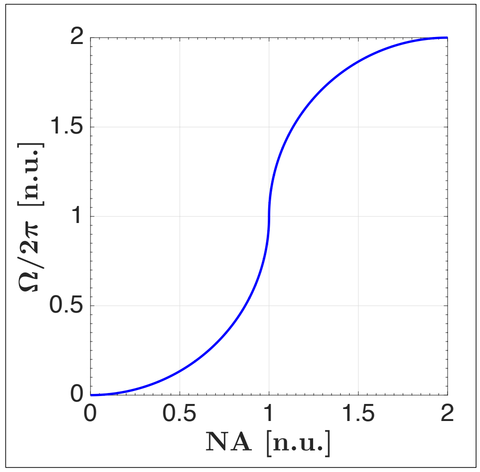

Figure S1. Relationship between the focusing solid angle Ω and the NA for a light cone, up to a 4π-illumination (NA = 2).

One could further express equation (S13) as the union of N incident beams sharing the same geometrical focus:

$$\Omega_N = \bigcup_{n=1}^{N} \Omega_n = \sum_{n=1}^{N}\left(\Omega_n - \sum_{m=1}^{m<n} \Omega_m \bigcap \Omega_n\right) = \sum_{n=1}^{N} \Omega_n - \sum_{n=1}^{N}\sum_{m=1}^{m<n} \Omega_{m,n}\,, \tag{S15}$$

where $\Omega_{m,n} = \Omega_m \bigcap \Omega_n$. We can generalize the NA expression up to 4π-illumination as:

$$\mathrm{NA} = \begin{cases} \sin\theta_{\mathrm{eff}} & \text{, for } 0 < \theta_{\mathrm{eff}} \leq \pi/2 \\ 2 - \sin\theta_{\mathrm{eff}} & \text{, for } \pi/2 < \theta_{\mathrm{eff}} \leq \pi \end{cases} \tag{S16}$$

with

$$\theta_{\mathrm{eff}} = \arccos\left(1 - \frac{\Omega_{\mathrm{eff}}}{2\pi}\right)\,. \tag{S17}$$

Hence, evaluating equation (S17) and inserting it in equation (S16) is a measure of the fill factor of the sphere illumination around the focus using the NA metric. Figure S1 shows the relationship between NA and Ω. Finally, one could re-write equation (S16) as:

$$\mathrm{NA} = \sin\theta_{\mathrm{eff}}\,[H(\theta) - 2H(\theta - \pi/2)] + 2H(\theta - \pi/2)\,, \tag{S18}$$

where H is the Heaviside function.

2. Linearly-polarized Super-Gaussian beam

In this section, we show the calculated focused field envelope of the six electromagnetic (EM) field components as obtained from the complex norm of the analytic signal (twice the sum over positive frequency components), using a 1 PW linearly-polarized (x-direction) Super-Gaussian beam of order 16 incident on the three focusing geometries (HNAP, OAP90 and TP).

2.1. HNAP

Figure S2 shows the focused field envelope obtained from a linearly-polarized beam incident on the HNAP geometry. The obtained fields are in full agreement with other works from the literature [1–9]. A strong dipolar-shaped E_z component with lobes positioned along the polarization axis is typical of non-paraxial beam focusing A slight ellipticity is observed for the field component in the polarization direction E_x, consistent with other works [7, 10].

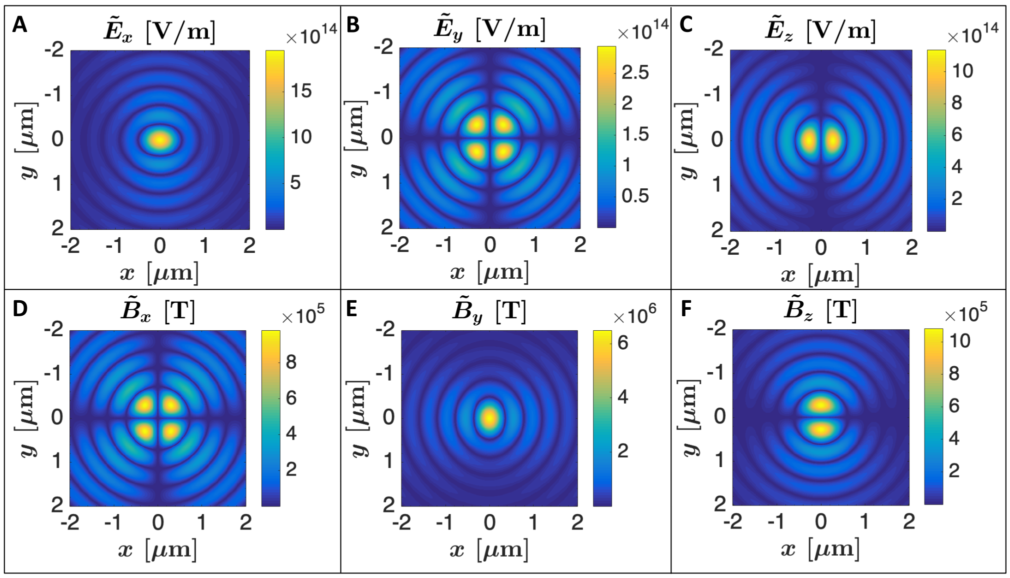

Figure S 2. Focused field envelope of the six electromagnetic (EM) field components evaluated in the focal plane ($z = 0$) and $t = 0$ (time of maximum intensity) for the HNAP reflector using an incident linearly-polarized (polarization along x axis) 1 PW (20 J in 20 fs) beam.

2.2. OAP90

Figure S3 shows the focused field envelope obtained from a linearly-polarized beam incident on the OAP90 geometry. The obtained fields are in full agreement with previous works on OAPs [5, 9]. In particular, the four lobes of component E_y seen for an on-axis parabola (see Figure S2.B) vanish into a dipolar shape when $\theta_{\text{off}} > 0$ as for this OAP geometry. A larger elliptical spot is observed for the 90° OAP.

2.3. TP

Figure S4 shows the focused field envelope obtained from a linearly-polarized beam incident on the TP geometry. The intensity distribution (see Figure 3 of the main document) exhibits two intensity lobes and an annular shape appear, with a local minimum in the center of the spot. This peculiar shape has been noted in the work of Sheppard [2] with a thin annular parabolic reflector and in the thesis of Person [11] using an ellipsoidal reflector. This effect is specific to an on-axis parabola section with $\theta > 90°$, and therefore it only applies to the TP reflector among the three presented in this work. More generally, the effect described in the following will be observed for any circularly symmetric reflector with obtuse focusing angles. It results from destructive interference

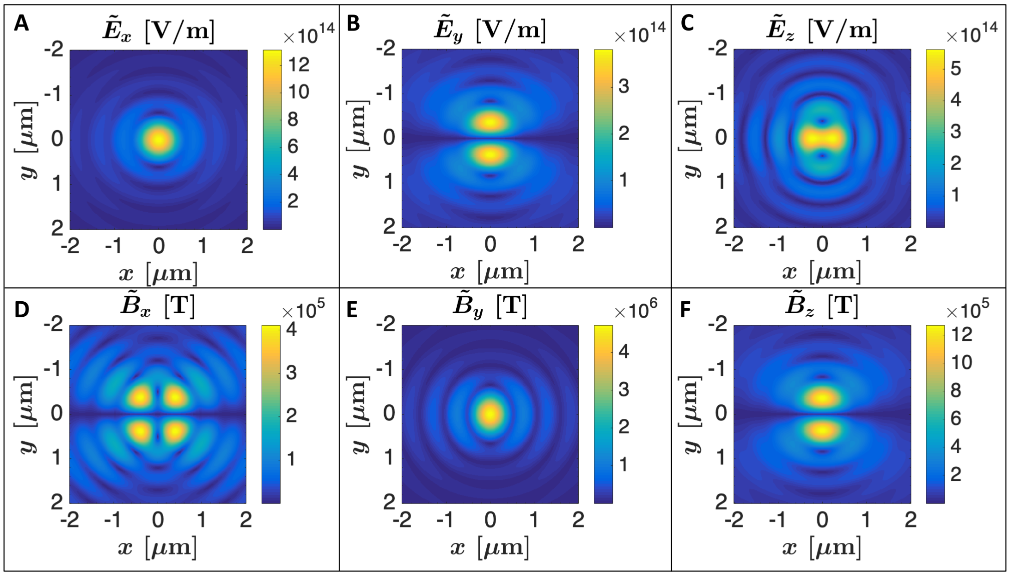

Figure S3. Focused field envelope of the six electromagnetic (EM) field components evaluated in the focal plane ($z = 0$) and $t = 0$ (time of maximum intensity) for the OAP90 reflector using an incident linearly-polarized (polarization along x axis) 1 PW (20 J in 20 fs) beam.

of the field component along the polarization direction, E_x and B_y here (see Figure S4.A and S4.E).

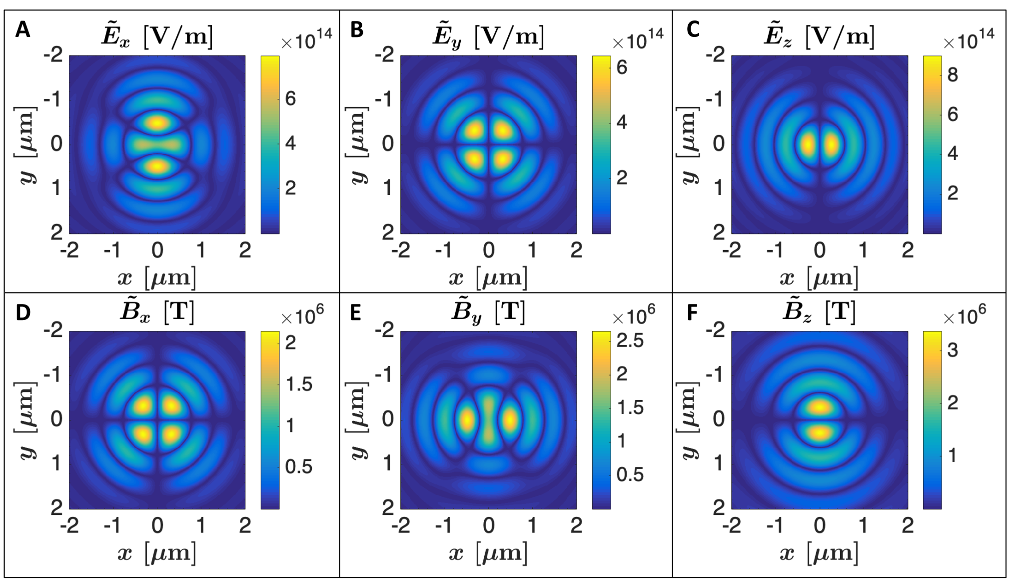

Figure S4. Focused field envelope of the six electromagnetic (EM) field components evaluated in the focal plane ($z = 0$) and $t = 0$ (time of maximum intensity) for the TP reflector using an incident linearly-polarized (polarization along x axis) 1 PW (20 J in 20 fs) beam.

3. Radially-polarized (TM_{01}) beam

In this section, we show the calculated focused field envelope of the six EM field components as obtained from the complex norm of the analytic signal (twice the sum over positive frequency components), using 1 PW radially-polarized (TM_{01}) incident beam on the three focusing geometries (HNAP, OAP90 and TP).

3.1. HNAP

Figure S5 shows the focused field envelope obtained from a radially-polarized beam incident on the HNAP geometry. The calculated field distributions are in agreement with other calculated fields from the literature [4, 6, 12–15].

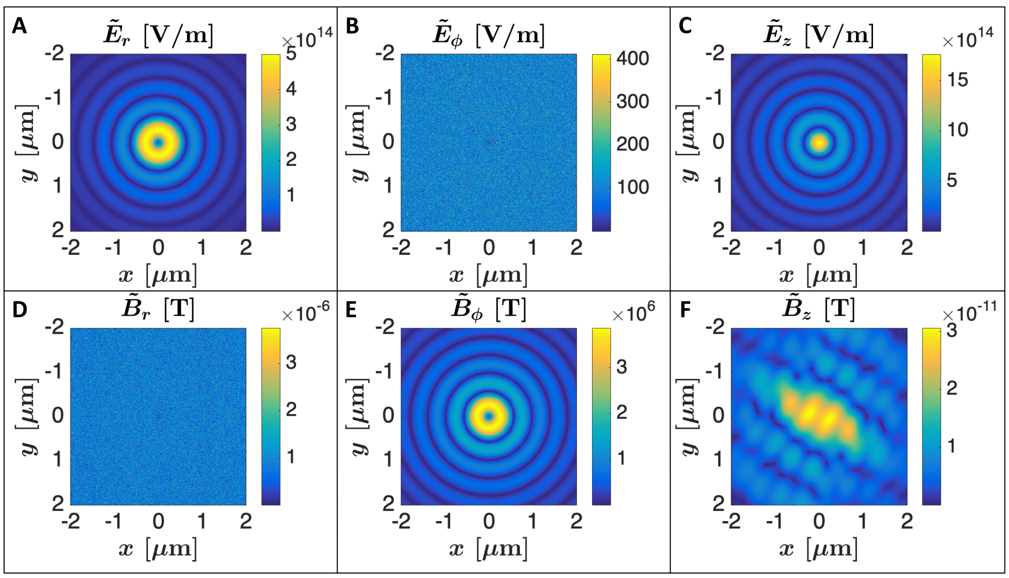

Figure S 5. Focused field envelope of the six electromagnetic (EM) field components evaluated in the focal plane (z = 0) and t = 0 (time of maximum intensity) for the HNAP reflector using an incident radially-polarized (TM_{01}) 1 PW (20 J in 20 fs) beam.

3.2. OAP90

Figure S6 shows the focused field envelope obtained from a radially-polarized beam incident on the OAP90 geometry. The fields are elliptical because the reflector has an asymmetrical shape. This focusing geometry used with a TM_{01} mode does not combine the fields optimally at the focus, yielding a larger spot. A non-negligible E_ϕ component emerges from the asymmetry, as observed in Figure S6.B.

3.3. TP

Figure S7 shows the focused field envelope obtained from a radially-polarized beam incident on the TP geometry. Note that the destructive interference seen with a linearly-polarized beam (see Figure S4) has now vanished. This is due to the same rotational symmetry between the incident field and the reflector preventing vectorial cancellation. The fields combine to produce a strong longitudinal E_z component following a typical Bessel-like distribution. The main difference between HNAP and TP is the π phase shift (*i.e.* reversed polarity) of their E_z component, however not seen here since we show the envelope of the signal (absolute value).

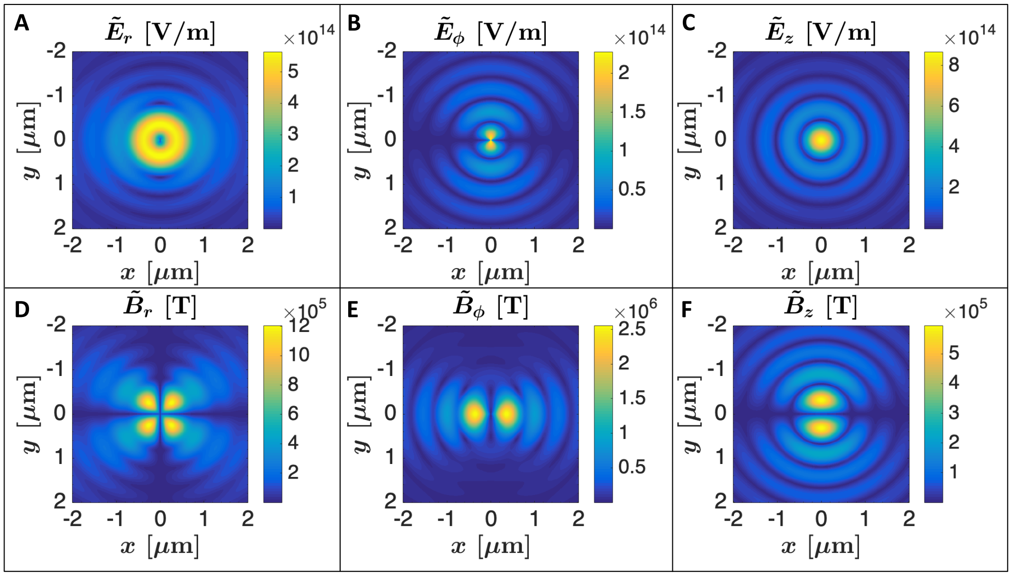

Figure S6. Focused field envelope of the six electromagnetic (EM) field components evaluated in the focal plane ($z = 0$) and $t = 0$ (time of maximum intensity) for the OAP90 reflector using an incident radially-polarized (TM_{01}) 1 PW (20 J in 20 fs) beam.

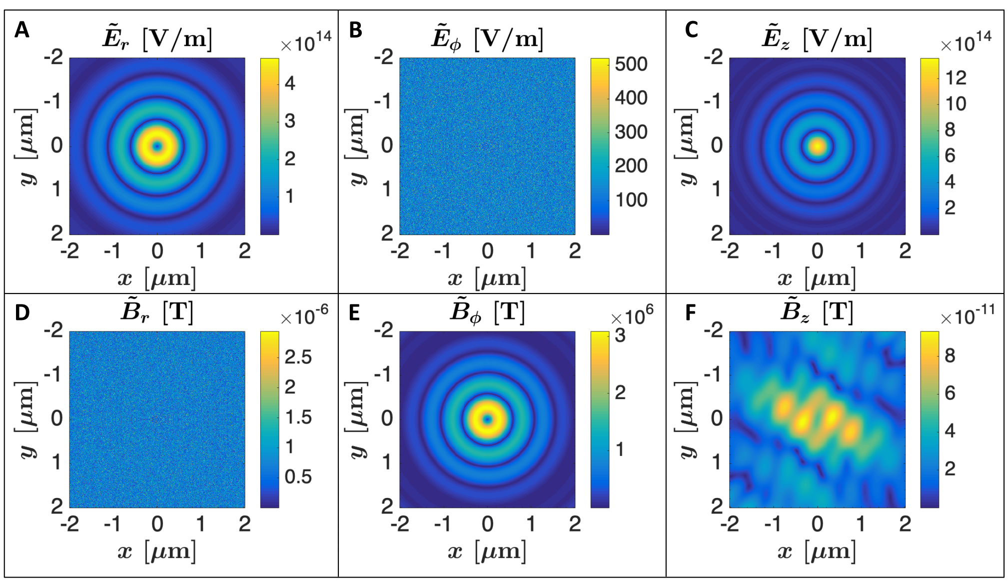

Figure S7. Focused field envelope of the six electromagnetic (EM) field components evaluated in the focal plane ($z = 0$) and $t = 0$ (time of maximum intensity) for the TP reflector using an incident radially-polarized (TM_{01}) 1 PW (20 J in 20 fs) beam.

4. Vector beam of order 2 using a Vortex Half-Wave Plate

Figure S8 shows the focused field envelope obtained from a linearly-polarized beam passed through an achromatic Vortex Half-Wave Plate (VHWP) of order $m = 2$ and then incident on the TP geometry. The destructive interference seen with a linearly-polarized beam (see Figure

S4) has now been completely inverted. The focused beam intensity distribution is now very similar to a linearly-polarized beam incident on the HNAP geometry (see Figure S2). We have verified (the numerical results are not displayed for simplicity) that a vector beam of order $m = 2$ incident on the HNAP geometry generates an intensity distribution equivalent to the TP with a linearly-polarized beam, as shown in Figure S4. These results confirm that the TP generates a tightly-focused vector beam of order ($m = 2$) and that a tightly-focused linearly-polarized beam (with $m = 0$) can be obtained from the combination of the VHWP and the TP geometry.

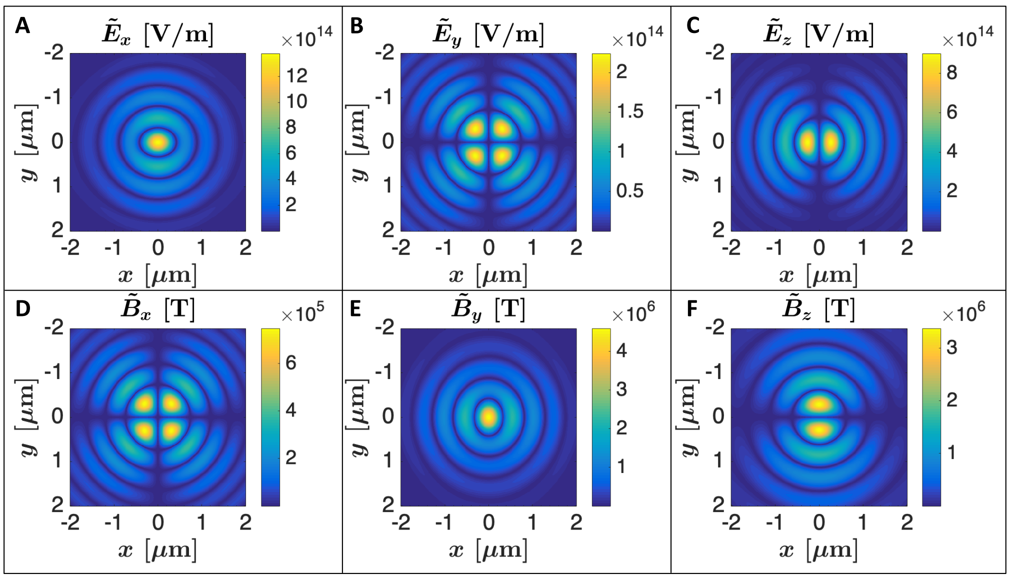

Figure S 8. Focused field envelope of the six electromagnetic (EM) field components evaluated in the focal plane ($z = 0$) and $t = 0$ (time of maximum intensity) for the TP reflector using an incident linearly-polarized (polarization along x axis) 1 PW (20 J in 20 fs) beam, and passing through an achromatic VHWP of order $m = 2$.

References

1. C. Sheppard, A. Choudhury, and J. Gannaway, "Electromagnetic field near the focus of wide-angular lens and mirror systems," IEE J. Microwaves Opt. Acoust. **1**, 129–132 (1977).
2. C. Sheppard, "Electromagnetic field in the focal region of wide-angular annular lens and mirror systems," IEE J. on Microwaves, Opt. Acoust. **2**, 163–166 (1978).
3. P. Varga and P. Török, "Focusing of electromagnetic waves by paraboloid mirrors. ii. numerical results," JOSA A **17**, 2090–2095 (2000).
4. M. Lieb and A. Meixner, "A high numerical aperture parabolic mirror as imaging device for confocal microscopy," Opt. Express **8**, 458–474 (2001).
5. S.-W. Bahk, P. Rousseau, T. A. Planchon, V. Chvykov, G. Kalintchenko, A. Maksimchuk, G. A. Mourou, and V. Yanovsky, "Generation and characterization of the highest laser intensities (10^{22} W/cm^2)," Opt. Lett. **29**, 2837–2839 (2004).
6. C. Stanciu, M. Sackrow, and A. Meixner, "High NA particle-and tip-enhanced nanoscale Raman spectroscopy with a parabolic-mirror microscope," J. microscopy **229**, 247–253 (2008).
7. S. G. Bochkarev and V. Y. Bychenkov, "Acceleration of electrons by tightly focused femtosecond laser pulses," Quantum Electron. **37**, 273 (2007).
8. K. Popov, V. Y. Bychenkov, W. Rozmus, and R. Sydora, "Electron vacuum acceleration by a tightly focused laser pulse," Phys. Plasmas **15**, 013108 (2008).
9. O. Vais and V. Y. Bychenkov, "Direct electron acceleration for diagnostics of a laser pulse focused by an off-axis parabolic mirror," Appl. Phys. B **124**, 1–13 (2018).

10. J. Dumont, F. Fillion-Gourdeau, C. Lefebvre, D. Gagnon, and S. MacLean, "Efficiently parallelized modeling of tightly focused, large bandwidth laser pulses," J. Opt. **19**, 025604 (2017).
11. S. M. Person, "Optical methods for nanoparticle detection and imaging," Ph.D. thesis, University of Rochester (2014).
12. S. Quabis, R. Dorn, M. Eberler, O. Glöckl, and G. Leuchs, "Focusing light to a tighter spot," Opt. Commun. **179**, 1–7 (2000).
13. J. Stadler, C. Stanciu, C. Stupperich, and A. Meixner, "Tighter focusing with a parabolic mirror," Opt. Lett. **33**, 681–683 (2008).
14. X. Gao, Q. Wang, M. Yun, J. Yu, H. Guo, and S. Zhuang, "Conditions for tighter focusing and higher focal depth of radially polarized vector beam." Opt. Appl. **42** (2012).
15. N. Lindlein, M. Sondermann, R. Maiwald, H. Konermann, U. Peschel, and G. Leuchs, "Focusing light with a deep parabolic mirror," arXiv preprint arXiv:1905.05997 (2019).